Hindawi
Shock and Vibration
Volume 2021, Article ID 2196838, 11 pages
https://doi.org/10.1155/2021/2196838

Research Article

Strain Rate Effect on Mechanical Properties of Cemented Backfill under Dynamic and Static Combined Loading

Xianglong Li,[1,2] **Zihao Tao**,[1,2] **Jianguo Wang**,[1,2] **Ting Zuo**,[1,2] **Jun Ma**,[1,2] **and Qiang Li**[1,2]

[1]*Faculty of Land Resources Engineering, Kunming University of Science and Technology, Kunming, Yunnan, China*
[2]*Yunnan Key Laboratory of China-German Blue Mining and Utilization of Special Underground Space, Kunming, China*

Correspondence should be addressed to Jianguo Wang; wangjg0831@163.com

Received 1 September 2021; Revised 26 November 2021; Accepted 16 December 2021; Published 31 December 2021

Academic Editor: Jun Wang

In order to study the influence of pillar stopping blasting on the stability of cemented backfill, the dynamic impact test under low strain rate (61.1~86.8 s^{-1}) was conducted on cemented backfill with two kinds of strength using three-dimensional coupled static-dynamic SHPB equipment. At the same time, the strain rate effect of failure mode, dynamic strength factor, and energy transfer of backfill were analyzed. The results show that when the cemented backfill was loaded under different strain rates in the initial three-dimensional static pressure environment, the pore compaction process was no longer obvious but directly entered the elastic deformation stage. Within the range of strain rates, the extreme value of dynamic intensity factor (DIF) of CTB_{230} was 6.8, while the extreme value of dynamic intensity factor of CTB_{310} specimen did not appear within the range of strain rates due to the improvement of the internal cementation force between particles. The fracture surfaces of specimens were perpendicular to the direction of load, and the failure mode was mainly the axial tensile failure, and the fracture surfaces were mostly close to the loading end. According to energy calculation, reflected energy accounts for 80.4%~86.6% of incident energy; dissipated energy, 5.5%~14.3%; transmitted energy, 5.3%~7.9%.

1. Introduction

The backfill mining method is widely used in underground mining projects because of its safety, economy, and environmental protection characteristics. With the working face advancing, to prevent the surrounding rock from caving and surface subsidence, mined rock is used as a filling aggregate to fill mined-out area, which provides a relatively safe working environment and reduces the economic cost of subsidence in mining enterprises [1]. As a kind of brittle material, cemented filling body showed a small structural damage under impact load, and the corresponding strain load time is short; then, this high strain rate induces the accumulation of the energy and stress concentration, which results in the generation, expansion, penetration of internal cracks, and structural failure under the action of the induced stress.

Split Hopkinson pressure bar (SHPB) impact test technology is generally used to study the dynamic characteristics of cemented backfill. Up to now, a large number of studies on the dynamic strength and failure energy of cemented backfill and similar-concrete materials have been carried out [2–16]. In Figure 1, the relevant dynamic compression experimental results are sorted out, and it can be seen that with the increase of strain rate, the dynamic strength of cemented backfill also increased. When the strain rate was low, the dynamic strength did not change obviously, but it changed obviously at a higher strain rate. In order to better describe the strength variation of materials similar to concrete under the effect of load, many scholars have proposed relevant dynamic strength criteria [17–19] based on experimental laws and concluded the variation equation of strength with strain rate. Wang et al. [20] studied the physical mechanism of dynamic strength of concrete-like

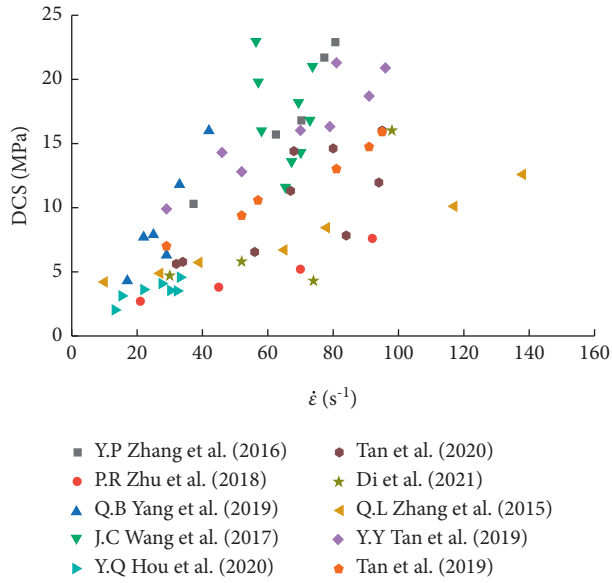

Figure 1: Research status diagram of the relationship between uniaxial dynamic compressive strength and strain rate of backfill material.

materials under different strain rates and showed that there was an extreme value of dynamic strength and obtained the S criterion of dynamic uniaxial compressive strength through theoretical deduction and experimental verification. The theoretical formula is as follows:

$$\mathrm{DIF} = 1 + \frac{F_{\max} F_0 \left(\dot{\varepsilon}/\dot{\varepsilon}\right)^{\xi/\ln 10}}{F_{\max} - F_0 + F_0 \left(\dot{\varepsilon}/\dot{\varepsilon}_0\right)^{\xi/\ln 10}}. \quad (1)$$

Here, ξ is the initial growth rate; $F_{\max}$ represents the maximum growth factor.

For the cement-like backfill material, when it is damaged, the consumed energy per volume is a constant [20]. According to this criterion, its dynamic strength will not increase infinitely with the strain rate but converge. Xu et al. [21] used the SHPB experimental technique to establish the empirical formula of dynamic strength change of backfill material. Besides, based on the fact that the increment of tensile strength and compressive strength caused by strain rate effect is equal, they proposed the inertia effect failure theory by conducting a dynamic tensile test. Yu et al. [3] analyzed the response of concrete-like materials under different strain rates. The results showed that the concrete-like material is not sensitive to the strain rate at low and medium strain rates, but its dynamic strength or yield stress is very sensitive at high strain rates. The S criterion of dynamic strength is used to modify the strain rate effect function of the classic Johnson-Cook constitutive.

When the cemented backfill material is subjected to different strain rates, the specimens will be tensile or experience splitting failure at different degrees, and this is a very complicated process. Song et al. [22] used the laboratory triaxial hydraulic test system to carry out cyclic loading and compression experiments on the cemented backfill material to explore the energy consumption mechanism during the failure process, deriving the calculation formula of damage in the three-dimensional state. Cheng et al. [9] used acoustic emission equipment to detect the ringing times of cemented backfill in the process of loading and explored the size effect of compressive strength and damage mode. Some scholars have explored the failure of cemented backfill materials under static and dynamic loads through numerical simulation technology and revealed the strain rate effect and energy dissipation law of backfill under load.

Based on this, in this paper, under different strain rates, the three-dimensional dynamic and static combined impact tests of cemented backfill with two kinds of strength were conducted, and the influence of different strain rates on the dynamic characteristics and failure mode of cemented backfill were explored. Furthermore, the strain rate effect of cemented backfill material was analyzed from the aspect of energy and damage.

2. Preparation of Specimen

In the actual backfill project, the cement content of the cemented backfill body ranged from 210 kg/m^3 to 280 kg/m^3. In this research, cemented backfill bodies with two different strengths, 230 kg/m^3 (represented by CTB_{230} in the following) and 310 kg/m^3 (represented by CTB_{310} in the following) were selected. The material ratio of these two cemented backfill bodies is shown in Table 1. The impact test under four different loading strain rates was carried out, while coaxial confining pressure was kept the same. The specimens with the size of 50 mm × 50 mm (diameter × height) were cured for 28 days under standard curing conditions. In order to ensure the uniform distribution of internal stress and strain when the specimen is impacted, the experiment requires a high smoothness on both ends of the specimen, and the parallelism is generally required to be within the range of 0.02 mm. The test piece was polished twice with a grinding machine, and the final length error of the test piece was controlled to be ±0.02 mm, and its roughness was about 0.02 mm (Figure 2).

3. Experimental Principle and Scheme

3.1. Test Equipment. The experiment was carried out on the SHPB experimental system with a diameter of 50 mm, as shown in Figure 3. The length of the incident rod and transmission rod is 2 m, and the bullet length is 0.35 m. During the experiment, different strain rates were realized by changing the impact pressure. In order to accurately and better analyze the strain rate effect of cemented backfill under three-dimensional conditions, all the tests were carried out under the same axial confining pressure. The SHPB experiment mainly collects the pulse values generated by the incident wave ε_I, reflected wave ε_R and transmitted wave ε_T in the impact process through strain gauges attached to the incident bar and transmission bar and then deduces the stress-strain relationship of the specimen according to the stress wave theory [23–25] following formulas (2)–(4):

Table 1: Proportion of specimens of cemented backfill with different strength.

Group	Tailings content (kg/m^3)	Cement content (kg/m^3)	Water (kg/m^3)	Contrast	Compressive strength (MPa)
CTB_{230}	1159	230	532	1 : 5	2.5
CTB_{310}	1058	310	532	1 : 3.5	5.0

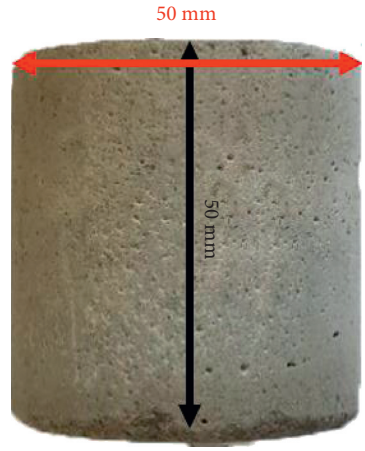

Figure 2: Specimen preparation.

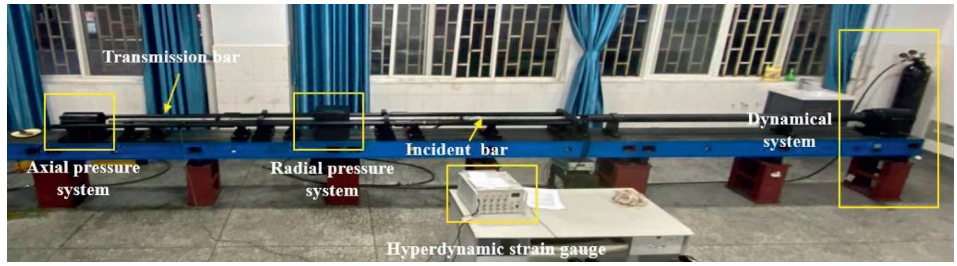

Figure 3: Triaxial coupled static-dynamic SHPB test equipment.

$$\sigma = \frac{AE}{A_0}\varepsilon_T. \tag{2}$$

In formula (2), σ is the stress generated when the specimen is impacted, MPa; A is the cross-sectional area of the incident bar; A_0 is the cross-sectional area of the specimen; ε_T is the strain in the transmission rod under the action of transmitted wave.

$$\varepsilon = -\frac{2C_0}{l_0}\int_0^t \varepsilon_R \mathrm{d}t. \tag{3}$$

In formula (3), ε is the strain generated when the specimen is impacted; C_0 is the elastic wave velocity of the incident bar; l_0 is the length of the specimen; ε_R is the strain in the incident bar under the action of reflected wave; t is time.

$$\dot{\varepsilon} = -\frac{AE}{A_0}\varepsilon_R. \tag{4}$$

In formula (4), $\dot{\varepsilon}$ quarter is the average strain rate of the specimens; E is the elastic modulus of the incident bar.

3.2. Test Strain Rates Loading. Different strain rate was realized by controlling the loading rate of the bullet. In order to obtain the experimental data while approximately keeping a loading with constant strain rate, a cylindrical brass plate with 5 mm thickness and the same diameter as the rod was used as the waveform shaper [26–29]. Under the condition of four different strain rates, triaxial coupled static-dynamic SHPB tests were carried out on cemented backfill with different strength (CTB_{230} and CTB_{310}), and the following typical waveforms were obtained as shown in Figure 4.

In Figure 4, U_R represents the reflected wave, U_I represents the incident wave, and U_T represents the transmitted wave. The impact rod used in the triaxial coupled dynamic and static combined impact test is spindle-shaped. The original waveform of data is in the shape of incident wave U_I and reflected wave U_R. Figure 4 shows the original waveforms of cemented backfill with the same material under the action of different strain rates. It can be seen that the absolute value of the peak incident wave was 0.13 mv when the strain rate was 62.1 s^{-1} and 0.21 mv when the strain rate was 82.1 s^{-1}. It can be seen that the U_I amplitude at different strain rates is proportional to the strain rate, and the width of

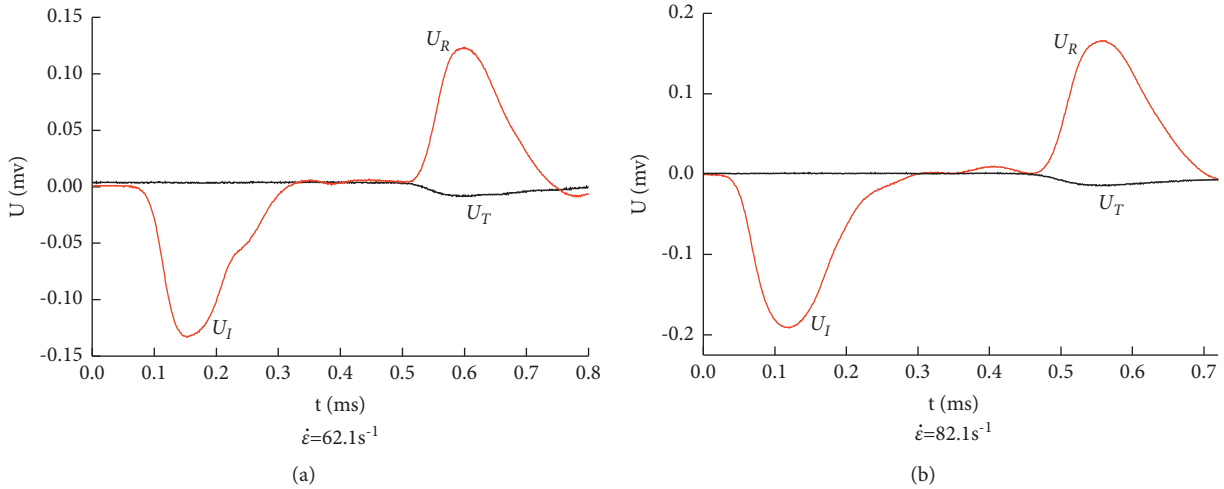

Figure 4: Typical waveforms at different strain rates.

U_I is related to the length of the bullet. The longer the bullet length, the wider the U_I width.

The experimental technique of SHPB is based on two basic assumptions: one is the one-dimensional stress wave hypothesis, which is basically true in the impact system with a bar diameter of 50 mm; the other is the specimen uniformity hypothesis under certain conditions. The wave impedance ratio of the test sample to Hopkinson bar material β has a significant effect on the stress balance; wave impedance $\sigma = \rho^* C_0$ (ρ is the specimen density, C_0 is the specimen wave velocity, and $C_0 = \sqrt{E/\rho}$, ρ is the specimen density). When $\beta > 1/100$ and the reflected stress wave is less than 10 times, the relative stress in the sample can be reduced to a low level, and the stress balance can be achieved inside the specimen.

Figure 5 shows the stress balance test curve of cemented backfill, namely, the superposition test of the stress at the incident end and the stress at the transmission end of the specimen. The stress at the incident end refers to the stress generated when the stress wave initially acts on the specimen, and the stress at the transmission end refers to the stress generated when part of the stress wave passes through the specimen. After the specimen was subjected to impact load, different degrees of internal and external damage occurred, and part of the energy was consumed. Therefore, there exists a certain deviation between the transmission stress curve and "incident + reflection" stress curve, as shown in Figure 5, in which the positive stress represents compressive stress, and the negative stress represents tensile stress [28–30]. Moreover, the reflected stress wave was mainly negative, that is, tensile stress, but positive at the end mainly because the specimen of cemented backfill body still had a certain residual strength. When the incident stress decreased, the elastic potential energy stored in the specimen was released and transferred to the bar, and a small amount of stress spring back occurred, indicating that the specimen satisfied the one-dimensional stress wave hypothesis and uniformity hypothesis under the strain rate.

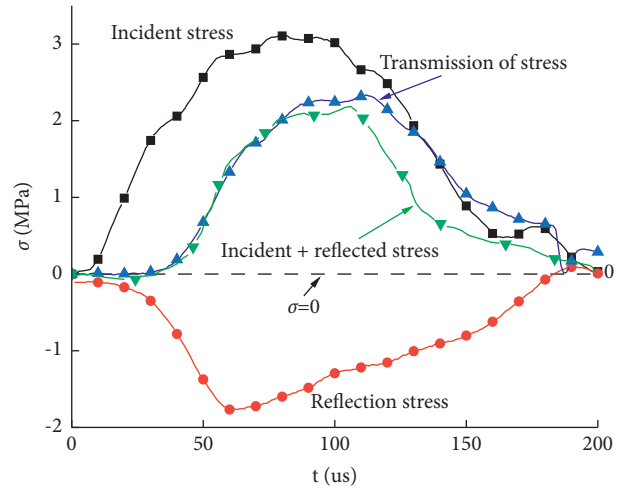

Figure 5: Stress balance test of cemented backfill.

In order to simulate the downhole pressure environment, the axial pressure ($P_i = 1.8$ MPa) and confining pressure ($P_a = 0.9$ MPa) were kept unchanged, the impact pressure (I_p) was set to be 0.40~0.55 MPa, and the strain rate was controlled in the range of 61.1~86.8 s^{-1} during the experiment.

4. Analysis of Dynamic Mechanical Properties

4.1. Dynamic Stress-Strain Curves. Under the impact of three-dimensional dynamic and static load, the dynamic strength of the cemented backfill has a positive relationship with the strain rate. As the strain rate increased, the dynamic strength of the material increased, and the plasticity was enhanced. Under the three-dimensional condition, before being subjected to a dynamic load, the specimen was subjected to a certain static load in both axial and radial directions, so that the original cracks in the specimen were closed and the elastic energy storage stage was completed. When the dynamic load was applied, the specimen directly

entered the elastic deformation stage, and linear deformation occurred. In the stress-strain curve, the front part of the curve is linear, which is different from the conventional SHPB impact test.

In Figure 6(a), CTB_{230} showed significant differences in dynamic strength under the action of different strain rates. When the strain rate was 62.3 s^{-1}, the dynamic strength of the specimen was 12.6 MPa. When the strain rate was 65.1 s^{-1}, the growth rate of the dynamic strength was about 33.6%. When the strain rate increased to 82.2 s^{-1}, the dynamic strength was 17.3 MPa and the growth rate was 3.5%. When the strain rate was 86.8 s^{-1}, the dynamic strength of the specimen is 17.7 MPa, and the growth rate is about 5.6%. It is indicated that when the strain rate of the backfill with cement content is relatively low, the strain rate effect of the material is more sensitive. When the strain rate is high, the strain rate effect of the material is less sensitive. When the strain rate was 62.3 s^{-1}, the slope of the front section of the $\sigma - \varepsilon$ curve was significantly higher than that under other strain rates, and the specimen entered the stress yield stage when the strain was about 0.005. Because the load acting on the specimen was relatively small at a lower strain rate, the specimen showed strong "resistance" in the early stage, and the slope in the front part of the curve was higher. With the continuous increase of the load, the energy in the specimen accumulated, and finally, the failure occurred.

By comparing these two Figures 6(a) and 6(b), it is found that CTB_{230} shows different failure strains under different strain rates. When the strain rate was 62.3 s^{-1}, the failure strain was about 0.005, and the failure strain was about 0.008 when the strain rate was 65.1 s^{-1}, 82.2 s^{-1}, and 86.8 s^{-1}. However, the failure strain of CTB_{310} at different strain rates remained unchanged at about 0.01. This is because that the CTB_{230} has a low content of cement, the cementation between the particles is low, and the dynamic response regularity under different strain rates is poor, while for CTB_{310}, the content of cement is relatively high, the cementation strength is strong, and the strain rate effect law is more obvious.

4.2. Dynamic Strength Factor Analyses. Under dynamic load with different amplitudes, the strain rate of material is different, and its strength is also different. The dynamic strength of cemented backfill under three-dimensional combined dynamic and static load did not increase infinitely with the increase of load. The S criterion characterizes the nonlinear dynamic strength of class concrete materials, indicating that the materials converge at high strain rates. DIF values of CTB_{230} and CTB_{310} specimens were calculated using formula (1), and the data were sorted out, as shown in Figure 7.

As shown in Figure 7, when the test strain rate ranged from 61.1 s^{-1} to 86.8 s^{-1}, the DIF value of the CTB_{230} specimen was fitted, and the change of DIF value conforms to the binomial law. When the strain rate ranged from 60.0 s^{-1} to 80.0 s^{-1}, the DIF value increased rapidly. When the strain rate was greater than 80.0 s^{-1}, the growth rate of DIF became slow and tended to be a constant value with the increase of strain rate, which conforms to the S criterion. By contrast, for the CTB_{310} specimen, the slope of the fitting curve of the DIF basically did not change with the strain rate. The damage of the specimen was caused by the external energy acting on the inside of the specimen, causing the energy to concentrate in the material particles. When the energy reached a certain threshold, the specimen reached the peak strength of the material. Because the cementation force between particles of CTB_{310} is higher than that of CTB_{230} specimen, when the strain rate is between 61.1 s^{-1} and 86.8 s^{-1}, the acting energy is not enough to reach the failure energy. Therefore, the slope of the curve changes little, and the DIF value does not show a peak.

5. Failure Behavior of Cemented Backfill under Different Strain Rates

5.1. Failure Characteristics. The typical failure modes of CTB_{230} and CTB_{310} specimens at different strain rates are shown in Figure 8.

Under triaxial coupled static-dynamic combined impact, with the increase of strain rate, the crushing degree of cemented backfill became higher, and the macroscopic cracks became more obvious. When the strain rate was 61.1 s^{-1}, visible macroscopic cracks appeared in the specimen. Because the specimen had been subjected to a certain radial and axial static load before subjecting to dynamic load, the internal cracks began to expand and penetrate under the action of tensile stress, a complete failure plane was developed inside, and the direction of the failure plane was perpendicular to the direction of dynamic load. The splitting tensile failure mode is obviously different from the conventional uniaxial SHPB test [31–35], and tensile failure occurs mainly in the specimens. As the strain rate continued to increase, the specimen produced multiple failure surfaces under the action of tensile stress, and most of the failure surfaces were inclined to the impact end, which finally formed axial layered failure. Due to axial pressure and confining pressure, the stress released at the crack inside the specimen was guided by axial and radial stress when the specimen was subjected to dynamic load. At the same time, the axial confining pressure was applied to make the specimen denser, which led to a larger failure lumpiness of cemented backfill in the triaxial coupled static-dynamic combination SHPB test than in the conventional SHPB test. At 62.3 s^{-1}, a macroscopic tensile crack surface was generated on the side of the CTB_{230} specimen, while the overall structure changed little and still had a certain bearing capacity. When the strain rate was greater than 65.1 s^{-1}, two macroscopic tensile cracks appeared, and the silty failure occurred. This may be due to the poor uniformity during the preparation of specimens. For the CTB_{310} specimen, when the strain rate was less than 81.0 s^{-1}, only one visible tensile crack was produced, and the specimen kept integrity. When the strain rate was greater than 81.0 s^{-1}, two macroscopic fractures appeared, leading to complete loss of bearing capacity. With the increase of strain rate, the load strength of the specimen also increases, so the failure degree of the specimen also increases. Due to the difference in cement

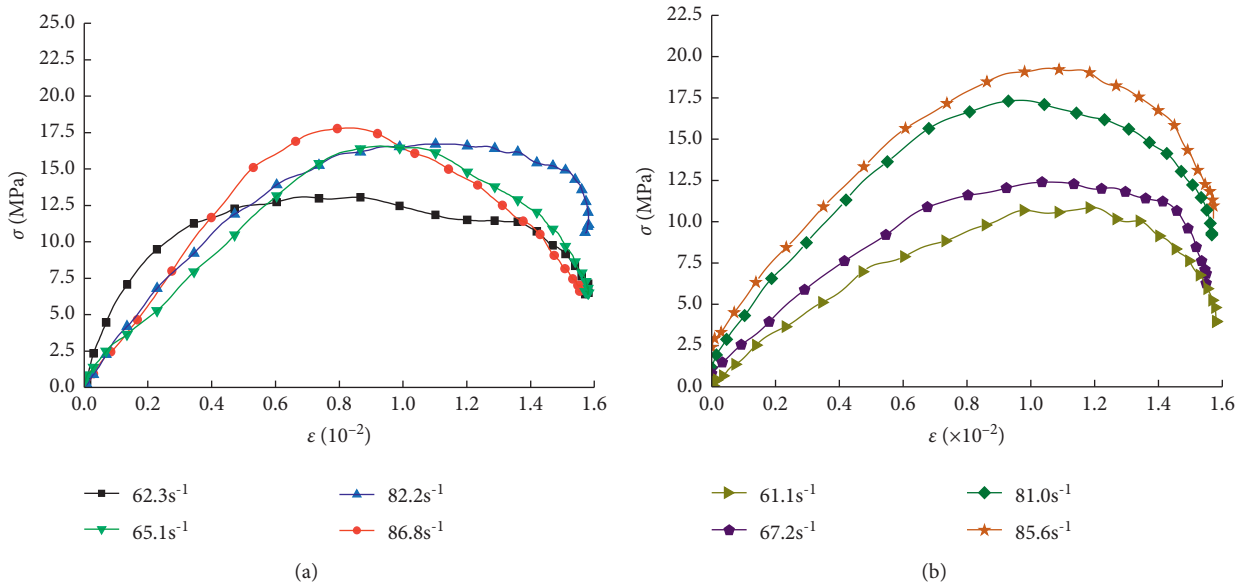

Figure 6: Stress-strain curves of cemented backfill under different strain rates. (a) CTB_{230}; (b) CTB_{310}.

content, the cementation strength between CTB_{230} particles is less than that of CTB_{310}, and the damage degree of CTB_{230} is significantly higher than that of CTB_{310} at the approximate strain rate.

5.2. Failure Energy Analyses. In order to better analyze the failure law of cemented backfill in a three-dimensional dynamic and static combined impact test. According to the SHPB experimental data processing principle [36, 37], the experimental data are integrated into Table 2. IP represents the impact pressure of the test, Φ represents the diameter of the specimen, H represents the height of the specimen, E_I represents the incident energy, E_R represents the reflection energy, E_T represents the transmission energy, E_A represents the dissipation energy, E_D represents the energy dissipation density, $\dot{\varepsilon}$ represents the test strain rate, DCS represents the peak strength of the specimen, and GLSp represents the peak strain when the specimen is damaged.

In the triaxial coupled static-dynamic combination SHPB test system, the energy comes from the bullet's kinetic energy, and it propagates in the bar in the form of a stress wave when it hits the incident bar. As shown in Figures 9(a) and 9(b), with the increase of experimental strain rate, the reflected energy in the system also increased, accounting for about 80% of the incident energy. On the contrary, the transmitted energy and dissipated energy changed little. This is because the filling material is relative to rock or other materials, in which there are a large number of primary pores even under the effect of axial confining pressure. When the stress wave acts on the specimen, it is difficult for the stress wave to pass through the holes and cracks, most of the stress wave is reflected into the incident bar in the form of reflected energy, but only a small part of the stress wave passes through the specimen and acts on the transmission bar. Therefore, the incident and reflected energy are high in the whole process, while the permeable and dissipated

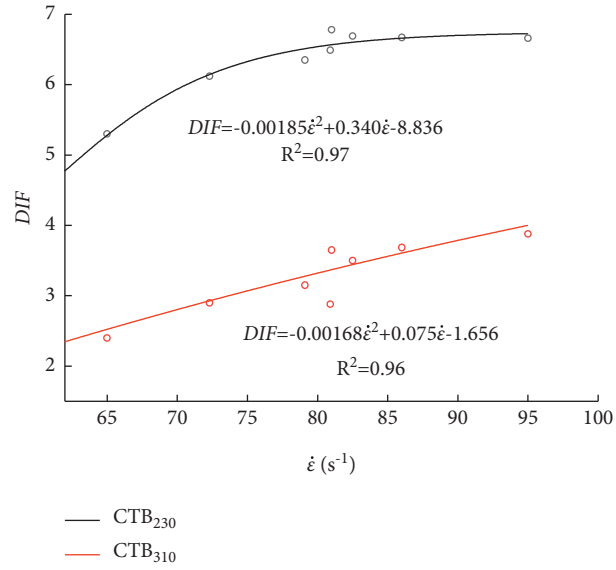

Figure 7: DIF values under different strain rates in three-dimensional dynamic and static combined impact tests.

energy is low. Besides, under the condition of a similar strain rate, the dissipated energy of the CTB_{310} specimen is higher than that of the CTB_{230} specimen. This is because the cementation force between particles in the CTB_{310} specimen is higher than that of CTB_{230}, and the failure energy of CTB_{310} specimen is higher. The ratio of transmitted energy and dissipated energy to incident energy reflects the characteristics of the material during the impact. This ratio of CTB_{230} and CTB_{310} specimens was about 8% and about 5%, respectively. According to the Figure 9, when the strain rate ranged from 61.1 s^{-1} to 86.8 s^{-1}, the ratio of dissipated energy was higher than that of transmitted energy. Because the cemented backfill material is a multipore material, the energy is concentrated on the tip of the original pore crack

Figure 8: Failure modes of cemented backfill under different strain rates. (a) CTB_{230}. (b) CTB_{310}.

Table 2: Calculation results of three-dimensional dynamic and static combined impact energy of cemented backfill.

Specimen number	IP (MPa)	Φ (mm)	H (mm)	E_I (J)	E_R (J)	E_T (J)	E_A (J)	E_D (J·cm^{-3})	$\dot{\varepsilon}$ (s^{-1})	DCS (MPa)	GLSp
CTB_{230}-1	0.40	50.02	49.89	96.4	83.51	5.59	8.30	0.136	62.3	12.51	0.0163
CTB_{230}-2	0.45	50.00	50.04	121.1	102.73	8.29	10.08	0.133	65.8	16.08	0.0175
CTB_{230}-3	0.50	49.98	49.95	165.9	140.19	11.78	13.93	0.142	82.2	17.07	0.0235
CTB_{230}-4	0.55	50.05	49.99	207.1	173.76	16.36	16.98	0.173	86.8	17.96	0.0238
CTB_{310}-1	0.40	49.87	50.11	89.8	72.20	5.21	12.39	0.127	61.1	10.81	0.0159
CTB_{310}-2	0.45	49.94	49.87	131.6	107.25	8.55	15.80	0.162	67.2	12.02	0.0183
CTB_{310}-3	0.50	50.03	50.00	172.8	142.21	14.69	15.90	0.164	81.0	16.80	0.0227
CTB_{310}-4	0.55	50.06	50.10	210.7	181.41	11.18	18.11	0.184	85.6	19.08	0.0231

In order to avoid the contingency and discreteness of the test, each group of specimens should be tested three times and the average value should be taken.

when the stress wave acts on the specimen, which is used for the development and expansion of the pore crack. However, due to this large number of pore cracks, it is difficult for the energy to pass through the specimen, so the dissipated energy is higher than the transmitted energy.

Energy dissipation density is the ratio of the energy used for specimen destruction in the system to the volume of the specimen when the material fails, and it represents the difficulty of material destruction under this load [38–44]. As it can be seen in Figure 10, when the strain rate increased, the E_D of the two kinds of backfill bodies also tended to increase as a whole. The E_D of CTB_{310} is higher than that of CTB_{230} at similar strain rates. However, when the strain rate was about 62 s^{-1}, the E_D of CTB_{310} and CTB_{230} was 0.127 J·cm^{-3} and 0.136 J·cm^{-3}, respectively. It can be seen from Figure 8 that when the strain rate was about 62 s^{-1}, CTB_{230} specimen obviously showed macroscopic crack surface, and the system consumed more energy for failure. By contrast, the CTB_{310} specimen did not show a macroscopic failure under this strain rate due to its high strength, and the system consumed less energy for failure. At this strain rate, the E_D of CTB_{310} was lower than that of CTB_{230}.

6. Discussion

In this paper, under three-dimensional static and dynamic loads, the strain rate effect of mechanical properties of two kinds of cemented backfill was explored through laboratory tests and theoretical analysis. The dynamic strength factor, failure mode, and energy distribution law of cemented

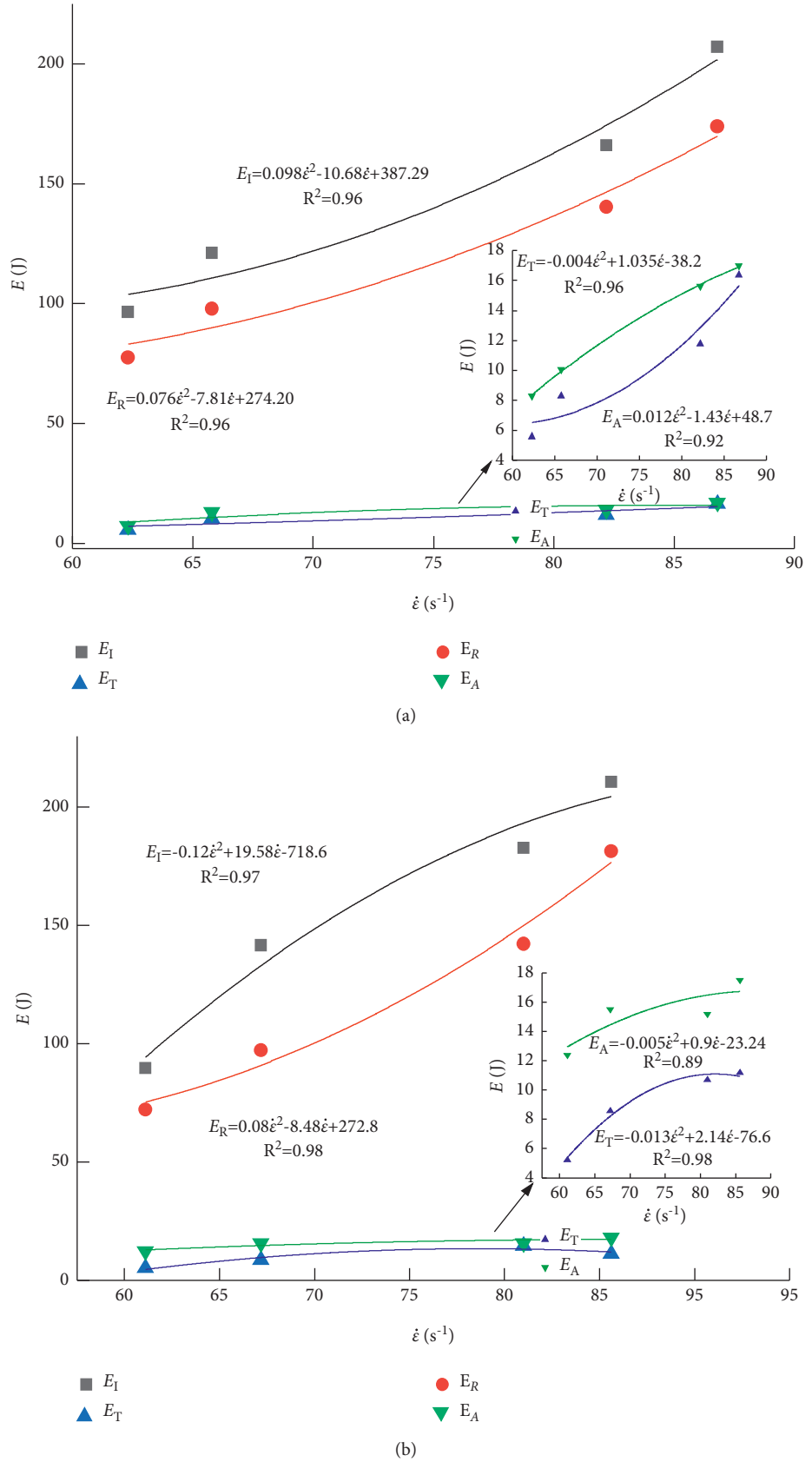

Figure 9: Relationship between incident, reflection, penetration and absorption energy, and strain rate. (a) CTB_{230}. (b) CTB_{310}.

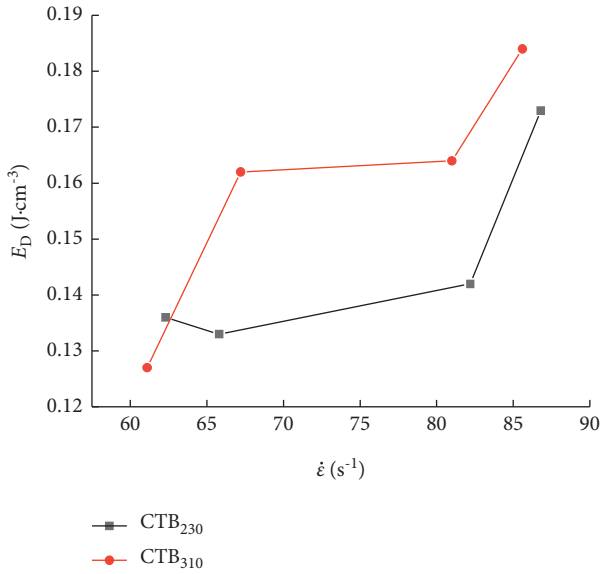

Figure 10: Relationship between energy dissipation density and strain rate.

backfill under different strain rates were discussed. Compared with the conventional uniaxial SHPB test, the three-dimensional dynamic and static combined impact model was adopted in the test, which can simulate the triaxial coupled static-dynamic of cemented backfill in the mine. At the same time, the dynamic mechanical parameters of the material under the triaxial coupled static-dynamic were obtained, which provides a reference for the relevant numerical simulation experiments. However, the test only used the three-dimensional dynamic and static combined impact equipment, which cannot completely simulate the real force state of the backfill. At the same time, only the backfill of two strengths was selected in the test process, and the backfill of other strengths was not considered. In the process of the test, the influence of the original crack and water content of the specimen on the test was not considered, which is a lack of comprehensiveness and diversity. Therefore, when mining the ore body adjacent to the filling body in the deep environment of high in situ stress, nonexplosive mining technology can be considered to reduce the influence on the stability of the cemented filling body [45–48].

7. Conclusions

In order to reflect the force of cemented backfill in the mine more truly, three-dimensional dynamic and static combination SHPB impact tests under different strain rates were conducted to study the dynamic mechanical properties, failure modes, and energy laws of cemented backfill with two kinds of strength, and the following conclusions can be drawn.

(1) In the three-dimensional dynamic and static combined impact test, due to the preloading of axial and radial static loads, the initial section of the stress-strain curve of the cemented backfill under different strain rates does not experience an obvious pore compaction process but directly enters the elastic deformation stage and finally yields and fails. When the loading strain rate is between 61.1 s^{-1} and 86.8 s^{-1}, the extreme DIF value of CTB$_{230}$ is 6.8, and the extreme DIF value of CTB$_{310}$ does not appear within the range of the strain rate due to the high interparticle bonding force.

(2) In three-dimensional dynamic and static combined impact tests, under different strain rates, the failure surfaces of specimens are all perpendicular to the loading direction, and the failure modes are mainly axial tensile failure, and the tensile fracture surfaces are primarily close to the loading end.

(3) The relationship between the incident, reflected, permeable, and dissipated energy of the cemented backfill with two strengths and the strain rate is established. With the increase of strain rate, the reflected energy in the system also increases, which accounts for about 80% of the incident energy. During the impact process, the dissipated energy of CTB$_{230}$ and CTB$_{310}$ specimens accounts for about 8%, and the transmitted energy accounts for about 5%. At the same time, the fitting degree of energy and strain rate data is higher than 0.9, indicating that the change of energy with strain rate accords with binomial relation. At the same time, the law of energy dissipation density under different strain rates is analyzed.

Data Availability

The data used to support the findings of this study are included in the article.

Conflicts of Interest

The authors declare that they have no conflicts of interest.

Authors' Contributions

T. Z. was responsible for the literature review, theoretical analysis, methodology, experimental process, data visualization, and original writing. J. W. was responsible for the test scheme modification and test operation guidance. X. L. and M. J. were responsible for writing analysis, thinking arrangement, and proofreading. All authors have read and agreed to publish the paper.

Acknowledgments

The authors are grateful for the financial support by the National Natural Science Foundation of China (no. 51934003).

References

[1] S. Xie, *Underground Mining of Metal Deposit*, pp. 4-5, Metallurgical Industry Press, Beijing, China, 2008.

[2] Y.-Y. Tan, X. Yu, D. Elmo, L.-H. Xu, and W.-D. Song, "Experimental study on dynamic mechanical property of cemented tailings backfill under SHPB impact loading,"

International Journal of Minerals, Metallurgy, and Materials, vol. 26, no. 4, pp. 404–416, 2019.

[3] S. S. Yu, Y. B. Lu, and C. Yong, "The strain-rate effect of engineering materials and its unified model," *Latin American Journal of Solids and Structures*, vol. 10, no. 4, pp. 833–844, 2013.

[4] Y.-Y. Tan, E. Davide, Y.-C. Zhou, W.-D. Song, and X. Meng, "Long-term mechanical behavior and characteristics of cemented tailings backfill through impact loading," *International Journal of Minerals, Metallurgy and Materials*, vol. 27, no. 2, pp. 140–151, 2020.

[5] Y. Zhang, X. Yang, and C. Chen, "Numerical simulation study on failure law of filling body under different impact velocity," *Chemical Minerals and Processing*, vol. 45, no. 7, pp. 39–41, 2016.

[6] Y. Zhang, X. Yin, and S. Yang, "Mechanical properties and energy consumption characteristics of cemented backfill under impact load," *Journal of Huazhong University of Science and Technology: Natural Science Edition*, vol. 48, no. 8, pp. 50–56, 2020.

[7] Q. Zhang, W. Yang, and S. Yang, "Experimental study on stability of cemented backfill with high density full tailings under dynamic load," *China Safety Science Journal*, vol. 25, no. 3, pp. 78–82, 2015.

[8] P. V. Nikolenko, S. A. Epshtein, V. L. Shkuratnik, and P. S. Anufrenkova, "Experimental study of coal fracture dynamics under the influence of cyclic freezing-thawing using shear elastic waves," *International Journal of Coal Science & Technology*, vol. 8, no. 4, pp. 562–574, 2021.

[9] A. Cheng, S. Dai, and P. Shu, "Study on creep characteristics and constitutive model of cemented backfill considering stress level and damage," *Journal of China Coal Society*, vol. 46, no. 2, pp. 439–449, 2021.

[10] Y. Wang, C. K. Liu, and X. F. Yi, "Study on the Fracture evolution of cemented backfill with cemented tailings," *Rock and Soil Mechanics*, vol. 41, no. 10, pp. 3365–3373, 2020.

[11] M. Wang, "Mechanical Characteristics of cemented backfill and surrounding rock Composite," *Journal of China Coal Society*, vol. 44, no. 2, pp. 445–453, 2019.

[12] J. Wang, Y. Fu, and Y. Hou, "Study on dynamic load impact failure of tailings backfill under different mix Ratio," *Mining Research and Development*, vol. 37, no. 3, pp. 8–13, 2017.

[13] Q. Yang, "Experimental study on mechanical properties of cemented filling under impact," *Modern Mining*, vol. 35, no. 3, pp. 84–86, 2019.

[14] P. Zhu, W. Song, and L. Xu, "Mechanical characteristics of cemented backfill under impact load," *Journal of Vibration and Shock*, vol. 37, no. 12, pp. 131–137, 2018.

[15] Z. Liu and X. Li, "Study on the stability of high stage filling body under blasting dynamic load," *Mining and Metallurgy Engineering*, vol. 24, no. 3, pp. 21–24, 2004.

[16] X. M. Wei, L. J. Guo, and C. H. Li, "Study on the Strength of cemented backfill," *Rock and Soil Mechanics*, vol. 39, no. s2, pp. 45–52, 2018.

[17] D. Zheng, W. Song, and S. Cao, "Investigation on dynamical mechanics, energy dissipation, and microstructural characteristics of cemented tailings backfill under SHPB tests," *Minerals*, vol. 11, no. 5, pp. 2–13, 2020.

[18] X. Liu, D. Fan, Y. Tan, and S. Song, "Failure evolution and instability mechanism of surrounding rock for close-distance parallel chambers with super-large section indeep coal mines," *International Journal of Geomechanics*, vol. 21, no. 5, pp. 158–174, 2021.

[19] X. Liu, S. Song, Y. Tan et al., "Similar simulation study on the deformation and failure of surrounding rock of a large section chamber group under dynamic loading," *International Journal of Mining Science and Technology*, vol. 31, no. 3, pp. 495–505, 2021.

[20] G. S. Wang, D. C. Lu, and X. L. Du, "Study on real dynamic strength and rate effect mechanism of concrete materials," *Engineering Mechanics*, vol. 35, no. 6, pp. 58–67, 2018.

[21] H. Xu and H. M. Wen, "Semi-empirical equations for the dynamic strength enhancement of concrete-like materials," *International Journal of Impact Engineering*, vol. 60, pp. 76–81, 2013.

[22] W. Song, J. Wang, and Y. Tan, "Physical energy consumption and damage characteristics of cutting and filling under triaxial loading and unloading," *Journal of China University of Mining and Technology*, vol. 46, no. 5, pp. 1050–1057, 2017.

[23] S. Cao, E. Yilmaz, and W. Song, "Strength and microstructural properties of cemented tailings backfill," *Minerals*, vol. 8, no. 8, pp. 205–225, 2018.

[24] H. Cheng, S. Wu, H. Li, and X. Zhang, "Influence of time and temperature on rheology and flow performance of cemented paste backfill," *Construction and Building Materials*, vol. 231, pp. 117–125, 2020.

[25] S. Yang, Z. Zhou, and Y. Zhao, "Study on dynamic mechanical properties of full tailings cemented backfilling impacted by cement-sand ratio," *Advances in Civil Engineering*, vol. 15, no. 7, pp. 128–137, 2018.

[26] F. Yang, H. Ma, L. Jing, and L. Zhao, "SciELO - Brazil - dynamic compressive and splitting tensile tests on mortar using split Hopkinson pressure bar technique Dynamic compressive and splitting tensile tests on mortar using split Hopkinson pressure bar technique," *Latin American Journal of Solids and Structures*, vol. 12, no. 4, pp. 147–158, 2015.

[27] A. Omi, A. Hosaka, M. Tomita et al., "Independently programmable frequency-multiplexed phase-sensitive optical parametric amplification in the optical telecommunication band," *Optics Express*, vol. 29, no. 14, Article ID 21683, 2021.

[28] H.-Y. Cheng, S.-Y. Wu, X.-Q. Zhang, and A.-X. Wu, "Effect of particle gradation characteristics on yield stress of cemented paste backfill," *International Journal of Minerals, Metallurgy and Materials*, vol. 27, no. 1, pp. 10–17, 2020.

[29] W. Sun, K. Hou, Z. Yang, and Y. Wen, "X-ray CT three-dimensional reconstruction and discrete element analysis of the cement paste backfill pore structure under uniaxial compression," *Construction and Building Materials*, vol. 138, pp. 69–78, 2017.

[30] S. Cao, E. Yilmaz, and W. Song, "Dynamic response of cement-tailings matrix composites under SHPB compression load," *Construction and Building Materials*, vol. 186, pp. 892–903, 2018.

[31] X. Li, X. Dong, and X. Yue, "Study on dynamic characteristics of vibration response transmissibility and its application in working mode analysis," *Journal of Vibration and Shock*, vol. 38, no. 9, pp. 62–70, 2019.

[32] Y. Wang, Y. Wang, and Y. Zhang, "Study on the Effect of the cemented backfill damage evolution," *Chinese Journal of Rock Mechanics and Engineering*, vol. 38, no. s1, pp. 3053–3060, 2019.

[33] A. P. Cheng and T. S. Wu, "Analysis of the dynamic strength of cemented backfill," *Chinese Journal of Rock Mechanics and Engineering*, vol. 13, no. 2, pp. 8–13, 1993.

[34] A. M. Bragov, A. K. Lomunov, D. A. Lamzin, and A. Y. Konstantinov, "Dispersion correction in split-Hopkinson pressure bar: theoretical and experimental analysis," *Continuum Mechanics and Thermodynamics*, vol. 115, no. 51, pp. 45–53, 2019.

[35] Y. Zhang and L. Yang, "A novel dynamic predictive method of water inrush from coal floor based on gated recurrent unit model," *Natural Hazards*, vol. 105, no. 2, pp. 2027–2043, 2020.
[36] S. Cao, W. Song, and E. Yilmaz, "Influence of structural factors on uniaxial compressive strength of cemented tailings backfill," *Construction and Building Materials*, vol. 174, pp. 190–201, 2018.
[37] G. Xue, E. Yilmaz, W. Song, and S. Cao, "Analysis of internal structure behavior of fiber reinforced cement-tailings matrix composites through X-ray computed tomography," *Composites Part B: Engineering and Science*, vol. 175, pp. 1–24, 2019.
[38] X. S. Liu, J. G. Ning, Y. L. Tan, and Q. H. Gu, "Damage constitutive model based on energy dissipation for intact rock subjected to cyclic loading," *International Journal of Rock Mechanics and Mining Sciences*, vol. 85, pp. 27–32, 2016.
[39] X. S. Liu, Y. L. Tan, J. G. Ning, Y. W. Lu, and Q. H. Gu, "Mechanical properties and damage constitutive model of coal in coal-rock combined body," *International Journal of Rock Mechanics and Mining Sciences*, vol. 110, pp. 140–150, 2018.
[40] Y. Yang, N. N. Zhang, and J. G. Wang, "A study on the dynamic strength deterioration mechanism of frozen red sandstone at low temperatures," *Minerals*, vol. 11, no. 12, p. 1300, 2021.
[41] Y. Yang, N. N. Zhang, and J. G. Wang, "Fracture morphology analysis of frozen red sandstone under impact," *Shock and Vibration*, vol. 2021, Article ID 4388132, 12 pages, 2021.
[42] J. G. Wang, T. Zuo, X. L. Li, Z. Tao, and J. Ma, "Study on the fractal characteristics of the pomegranate biotite schist under impact loading," *Geofluids*, vol. 2021, Article ID 1570160, 8 pages, 2021.
[43] Z. Y. Zhang, Q. Y. Qian, H. Wang, Y. H. Huang, J. G. Wang, and H. S. Liu, "Study on the dynamic mechanical properties of metamorphic limestone under impact loading," *Lithosphere*, vol. 2021, no. 4, Article ID 8403502, 2021.
[44] P. V. Nikolenko, S. A. Epshtein, V. L. Shkuratnik, and P. S. Anufrenkova, "Experimental study of coal fracture dynamics under the influence of cyclic freezing-thawing using shear elastic waves," *International Journal of Coal Science & Technology*, vol. 8, no. 4, pp. 562–574, 2021.
[45] S.-F. Wang, Y. Tang, X.-B. Li, and K. Du, "Analyses and predictions of rock cuttabilities under different confining stresses and rock properties based on rock indentation tests by conical pick," *Transactions of Nonferrous Metals Society of China*, vol. 31, no. 6, pp. 1766–1783, 2021.
[46] S. Wang, X. Li, J. Yao et al., "Experimental investigation of rock breakage by a conical pick and its application to non-explosive mechanized mining in deep hard rock," *International Journal of Rock Mechanics and Mining Sciences*, vol. 122, no. 2, Article ID 104063, 2019.
[47] S. F. Wang, L. C. Sun, X. B. Li et al., "Experimental investigation of cuttability improvement for hard rock fragmentation using conical cutter," *International Journal of Geomechanics*, vol. 21, no. 2, Article ID 06020039, 2021.
[48] S.-F. Wang, Y. Tang, and S.-Y. Wang, "Influence of brittleness and confining stress on rock cuttability based on rock indentation tests," *Journal of Central South University*, vol. 28, no. 9, pp. 2786–2800, 2021.